HHS Public Access

Author manuscript

*Anal Chem*. Author manuscript; available in PMC 2023 June 07.

Published in final edited form as:

*Anal Chem*. 2022 June 07; 94(22): 7901–7908. doi:10.1021/acs.analchem.2c00648.

# Multiplexed Analysis of the Cellular Uptake of Polymeric Nanocarriers

**Dheeraj K Agrohia**[1,‡],

**Peidong Wu**[1,‡],

**Uyen Huynh**[1],

**S Thayumanavan**[1,2,3,*],

**Richard W Vachet**[1,2,3,*]

[1]Department of Chemistry, University of Massachusetts Amherst, Amherst, Massachusetts 01003, United States.

[2]Molecular and Cellular Biology Program, University of Massachusetts Amherst, Amherst, Massachusetts 01003, United States.

[3]Center for Bioactive Delivery-Institute for Applied Life Sciences, University of Massachusetts Amherst, Amherst, Massachusetts 01003, United States.

## Abstract

Polymeric nanocarriers (PNCs) are versatile drug delivery vehicles capable of delivering a variety of therapeutics. Quantitatively monitoring their uptake in biological systems is essential for realizing their potential as next generation delivery systems; however, existing quantification strategies are limited due to the challenges of detecting polymeric materials in complex biological samples. Here, we describe a metal-coded mass tagging approach that enables the multiplexed quantification of PNC uptake in cells using mass spectrometry (MS). In this approach, PNCs are conjugated with ligands that bind strongly to lanthanide ions, allowing the PNCs to be sensitively quantitated by inductively-coupled plasma (ICP)-MS. The metal-coded tags have little effect on the properties or toxicity of the PNCs, making them biocompatible. We demonstrate that the conjugation of different metals to the PNCs enables the multiplexed analysis of cellular uptake of multiple distinct PNCs at the same time. This multiplexing capability should improve the design and optimization of PNCs by minimizing biological variability and reducing analysis time, effort, and cost.

## Graphical Abstract

*Corresponding authors: thai@chem.umass.edu, rwvachet@chem.umass.edu.
‡These authors contributed equally.

Supporting Information

Additional information, including the synthetic materials and methods, characterization results for the polymers used in this study, cytotoxicity assay results, and ICP-MS response factors can be found in the Supporting Information section. The Supporting Information is available free of charge on the ACS Publications website at DOI:

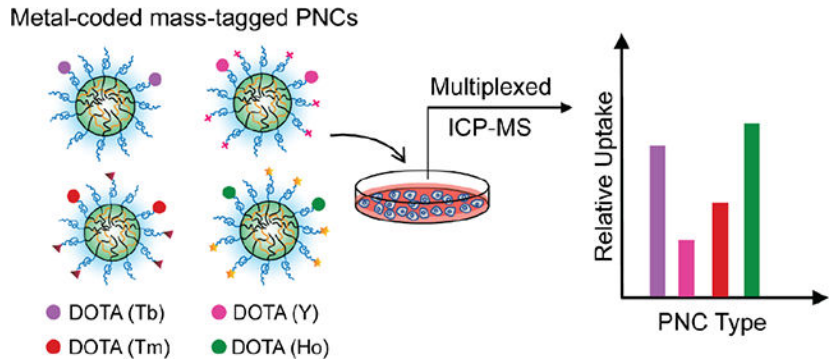


## Introduction

Nanocarriers (NCs) are increasingly popular as effective drug delivery vehicles, especially within the field of oncology.[1] They have the potential to improve the solubility, stability and pharmacokinetics of drug molecules.[2–4] So far, various kinds of NCs, including liposomes,[5,6] proteins,[7,8] polymers,[9–12] and metal-based[13–15] materials have been investigated to enhance overall efficacy and safety of conventional drug molecules. Among these NCs, polymer-based nanocarriers (PNCs) are promising delivery systems because of their facile synthesis and easy control over size, shape, charge, and surface functionality. Along with being made biocompatible and biodegradable, PNCs offer many other advantages including long circulation times,[16,17] stimuli responsive and controlled drug release,[18–20] and the ability to incorporate small drugs[21–23] and/or biologics.[24,25]

While numerous examples of efficacious and safe PNC systems have been reported, relatively few have been translated into clinical studies, indicating a gap between the technical and clinical development of PNCs. Some of this gap is due to the lack of methods to monitor PNCs *in vitro* and *in vivo* so that correlations between structural properties and biodistributions can be made. Large experimental variabilities associated with *in vivo* models, in particular, make it difficult to compare the efficacy of different PNC formulations. Moreover, ethical considerations dictate the use of fewer animals for the evaluation of PNCs. Hence, sensitive analytical methods that can quantitatively monitor multiple PNCs in a single set of experiments are desired to reduce time, effort, the number of animals, and to minimize experimental variability.

A variety of techniques, such as fluorescence imaging,[26–28] radiolabeling,[29–31] magnetic resonance imaging,[32,33] and electron microscopy[34,35] have been used to track PNCs in biological samples. Fluorescence methods are very commonly used, but these approaches suffer from quenching, intrinsic fluorescence interferences, poor quantitation, and limited multiplexing capabilities. Radiolabeling approaches suffer from stringent safety precautions, and there is a general move away from the use of radioactive elements in many fields of science. Magnetic resonance imaging has poor sensitivity and hence demands high loading of contrast agents. Electron microscopy methods have an inherent advantage in that they can be used without needing to chemically label PNCs, but this method is slow, not quantitative, and does not readily lend itself to multiplexing. Overall, existing techniques

lack the quantitative and multiplexing capability needed to simultaneously monitor multiple PNCs.

Because of its speed, sensitivity, and inherent multiplexing capability, mass spectrometry (MS) is beginning to be used to detect NCs in biological systems, including carbon,[36] lipid,[37,38] and metals-based NCs.[39–44] Matrix-assisted laser desorption ionization mass spectrometry (MALDI-MS) readily detects lipids[45] and hence has been used to detect liposomes[37] and cationic lipid based NCs.[38] Laser desorption ionization mass spectrometry (LDI-MS) has been utilized to measure carbon cluster ions as proxies of carbon-based NCs[36] and to detect surface coatings on intact AuNPs.[41,42] Inductively-coupled plasma mass spectrometry (ICP-MS) is widely used to monitor metal-based NCs.[43,44,46]

The applicability of MS to PNCs, however, has been limited due to the challenges of detecting polymers directly in complex biological samples. In this work, we describe the development of metal-coded mass tags (MMTs) that enable multiple PNCs to be detected and quantified in a single experiment. These MMTs consist of a cyclic polyaminocarboxylate ligand known as DOTA (1,4,7,10-tetraazacyclododecane-1,4,7,10-tetraacetic acid) that complexes strongly to wide range of metal ions.[47] Such DOTA ligands and other structurally similar complexation agents have been used in quantitative proteomics,[48–50] imaging mass cytometry for biomarker detection,[51–53] as part of contrast agents in magnetic resonance imaging,[54–56] and to track organic and inorganic nanoparticles via radioactive elements.[29,57,58] To the best of our knowledge, however, such MMTs have not been incorporated into PNCs to enable their detection in biological samples. Here, using two types of nanogel (NG) PNCs as testbeds, we demonstrate that MMTs can be installed in PNCs without significantly altering their size, charge, or uptake properties. We then illustrate the multiplexing capabilities of these MMTs by quantifying the relative cellular uptake of NG PNCs having different targeting functionality (Figure 1).

## Experimental Section

The detailed synthetic methods and characterization results for all the polymers used in this work can be found in Supporting Information.

### Conjugation of the MMTs to the polymers

Polymer P1 (Scheme S1) or polymer P6 (Scheme S2) was dissolved into anhydrous dimethylformamide. Then, excess of triethylamine (TEA) was added, and the solution was stirred for 30 min. After activating the amines with TEA, 3 equivalents of DOTA-mono-NHS tris (*t*-Bu-ester) per amine were added, and the reaction mixture was stirred for 24 h. The mixture was then dialyzed (Spectra/Por, ThermoFisher Scientific, MWCO = 3.5kDa) against a 4:1 mixture of dichloromethane (DCM):methanol for 2 days. The solvent was removed under vacuum, and resultant P2 or P7 polymer (Schemes S1 and S2) was characterized by NMR (Figure S1 and S2) to find the characteristic *t*-Bu peak (~1.5 ppm) of the added DOTA group.

Removal of the *t*-Bu groups on the DOTA moieties was accomplished by dissolving P2 or P7 into a 1:1 mixture of trifluoroacetic acid (TFA):DCM and stirring the mixture overnight.

Then, the reaction mixture was extracted three times with cold ether to precipitate the pure polymers of P3 or P8 (Schemes S1 and S2) and remove TFA and *t*-Bu-OH. The resulting P3 and P8 polymers were characterized by the loss of the *t*-Bu peak (~1.5 ppm) in NMR (Figure S1 and S2).

Metal complexation of the DOTA-tagged polymers was achieved by the following general procedure. First, the required amount of P3 (or P8) (0.1–3 mg) was dissolved into water (or water with a small amount of dimethylsulfoxide), and the metal chloride of interest (2 equivalents with respect to the number of DOTA groups in the polymer) in a 100 mM ammonium acetate buffer (pH=5.5) was added and stirred overnight at room temperature. Then, a 1:1 equivalent of $Na_2EDTA$ to metal chloride was added and stirred for 15 min to sequester free metal ions. Finally, the reaction mixture was purified by three ultra-centrifugal filtration procedures using 3 kDa molecular weight cutoff filters (Amicon).

## Formation and characterization of the cross-linked NG assemblies

The experimental details for forming and characterizing the NG assemblies can be found in the supporting information.

## Cell culture and NG uptake experiments

HeLa, MCF-7, and HEK293T cells lines were grown in growth media comprised of Minimum Essential Medium supplemented with 10% fetal bovine serum and 1% antibiotic solution (10,000 units/mL of penicillin and 10,000 μg/mL of streptomycin). All cell cultures were nurtured under humidified conditions with 5% $CO_2$ at 37 °C. Cells (~$0.5 \times 10^6$) were plated into 24-well plates 24 h prior to NG treatment. After plating, the growth media was replaced with media containing the NG(s) of interest (0.1 mg/ml for the uniplex studies and a total of 0.4 mg/mL for the multiplexed studies). After 24 h of treatment with the NG(s), the cells were washed three times with ice cold phosphate-buffered saline (PBS) to remove NGs that were not taken up into the cells. The cells were then harvested into 15 mL centrifuge tubes and prepared for ICP-MS analysis.

## ICP-MS sample preparation and analysis

To measure the amount of metal incorporated into the polymers, fixed amounts of samples and standard Ir solutions were treated with *aqua regia* (highly corrosive, use with high caution) overnight. The samples were then diluted to obtain 5% *aqua regia*. A series of calibrant solutions of the metal of interest along with Ir as an internal standard were prepared in 5% *aqua regia*.

In harvested cell samples, an Ir solution was again added as an internal standard, and the cell mixtures were digested using 100 μL of a 3:1 mixture of $HNO_3$ and $H_2O_2$ and sonicated for 1 h. After sonication, *aqua regia* was added and tubes were again sonicated to further digest the cell samples. Finally, the digested mixture was diluted with deionized water to give a ~5% *aqua regia* solution. To generate response factors for quantification purposes, control cell lysates were spiked with a constant amount of Ir (as an internal standard) and increasing concentration of the NG of interest.

All samples were measured on a PerkinElmer NexIon300X ICP mass spectrometer. The instrument was operated under following conditions: plasma argon flow = 16.5 L/min; nebulizer gas flow = 1.1 L/min; rf power = 1600 watts and dwell time = 50 ms.

## Results and Discussion

We first tested if MMTs could be used as proxies to monitor cellular uptake of PNCs. A random amphiphilic polymer (P1) consisting of amine (6%), oligoethylene glycol (30%), and pyridyl-disulfide (64%) as repeating units was designed, synthesized, and used as a model polymer system (Scheme S1). Nanogels (NGs) constructed from this polymer have been used previously to deliver small chemotherapeutics,[59,60,61] nucleic acids,[62] and proteins[63,64] to cells. MMTs were attached to the polymer, and then the NGs were fabricated (Scheme S1). First, tris-*t*-Bu-DOTA was conjugated to P1 and confirmed by NMR (Figure S1). Next, the *t*-Bu-ester groups of the polymer (i.e. P2 in Scheme S1) were hydrolyzed, and the resulting P3 was complexed overnight with $Ho^{3+}$ at a pH of 5.5. Excess free $Ho^{3+}$ was removed using $Na_2EDTA$, followed by ultra-centrifugal filtration. The number of washes and filtration steps required to remove noncomplexed $Ho^{3+}$ was determined by comparing the $Ho^{3+}$ concentrations associated with P3 and the control polymer P0 (Figure 2a, b). A total of three ultra-centrifugal washing cycles was found to be sufficient to remove non-specifically bound $Ho^{3+}$. The amount of attached $Ho^{3+}$ was determined to be ~0.65 weight% of P3, where weight% = (ng of attached $Ho^{3+}$/ ng of P3) × 100. After complexation and washing, DTT was used to cross-link P4 (Ho) and create the $Ho^{3+}$-coded NG (Ho-NG).

The cellular uptake of Ho-NG was tested with HeLa cells (~$0.5 \times 10^6$ cells). After 24 hours of incubation with Ho-NG (0.1 mg/mL), cells were washed three times with PBS, which was found to be the optimal washing conditions (Figure S3). The total Ho concentration in the cells was then quantified by ICP-MS to determine the uptake of the NGs. The ICP-MS response factor for Ho-NG was determined by spiking different Ho-NG concentrations into HeLa cell lysate to establish a calibration curve. From three replicate measurements, we found the percent cellular uptake of Ho-NG to be 0.77 ± 0.03 %. While NGs like this one have been used to successfully deliver small drugs and biologics to cells,[59,60,62–66] these are the first quantitative measurements of the uptake of these NGs.

Before evaluating the ability of the MMTs to enable multiplexed analysis of several different NGs, it was crucial to first make sure that the MMTs themselves do not affect the biophysical properties of the NGs. So, we next investigated the optimal amount of MMTs that could be installed on the polymers without affecting the NG's properties. To control the amount of MMTs in the NGs, we synthesized an amphiphilic block copolymer (P6, Scheme S2) consisting of oligoethylene glycol and pyridyl-disulfide moieties, as repeating units, and terminated the polymer with an amine group, so that each polymer chain could accommodate exactly one MMT group. These block co-polymers provided better control over the percentage of MMT groups present in each nanogel as compared to the random co-polymer P4 (Ho), and all subsequent cell-based studies were performed with these polymers. A $Tm^{3+}$-coded mass tag was then attached to P6 via the amine (Figure S2 and Scheme S2) to create polymer P9 (Tm), and the MMT-polymer was purified as described above (i.e. Figure 2a). Then, the $Tm^{3+}$-coded polymer P9 (Tm) was mixed with a control

polymer, P10, in different ratios and the resulting polymeric mixtures were cross-linked to obtain $Tm^{3+}$-coded NGs with MMT percentages ranging from 1 to 100% (Figure 3a). DLS measurements of these resulting NGs indicate that the different MMT percentages have relatively little influence on their zeta potentials and sizes (Figure 3b, c).

The influence of different MMT percentages on NG cellular uptake was studied by incubating NGs (formulated from different ratios of P9 (Tm) and P10) using HeLa cells. After 24 h of incubation, cells were washed three times with PBS, and the total metal was quantified by ICP-MS to determine the uptake of the NGs. Response factors for each NG were generated (Figure S4) and used to quantify their % uptake. As shown in Figure 3d, uptake is relatively constant for NGs having up to 10% MMT. Further increases in the MMT percentage result in significant changes in uptake, causing us to conclude that up to 10% MMT can be used without substantially influencing NG properties or uptake efficiency. For further studies, we chose to incorporate 10% MMT to maximize detection sensitivity.

Multiplexed screening of the NGs with the MMTs requires the complexation of different metal ions that range in size. So, we investigated the cytotoxicity of the 10% MMT-conjugated NGs with different complexed metals, including $Ho^{3+}$, $Tm^{3+}$, $Tb^{3+}$ and $Y^{3+}$. We chose rare earth metal ions for several reasons. (i) They have no biological background, allowing them to be detected at very low levels; (ii) their formation constants are very high ($> 10^{20}$), leading to great stability in biological samples; and (iii) they have almost no isobaric interferences during ICP-MS analyses, which allows for better measurement precision. Four NGs based on P10 and metal-coded polymer P9 (P9 coded with $Ho^{3+}$, $Tm^{3+}$, $Tb^{3+}$ or $Y^{3+}$), each with 10% MMT and complexed with a different metal ion, were fabricated and incubated with HeLa, HEK293T, and MCF-7 cells at polymer concentrations ranging from 0.1 – 1.0 mg/mL. After 48 h of incubation, there is no significant loss of cell viability as determined using the Cell Titer Glo assay (Figure S5), indicating that NGs with 10% MMT density and a variety of light ($Y^{3+}$) and heavy ($Tm^{3+}$, $Ho^{3+}$ and $Tb^{3+}$) rare earth metals causes no cytotoxicity.

The reliability of using the MMTs with different complexed metals to quantitate the cellular uptake of PNCs can be further demonstrated by assessing the uptake of NGs with different targeting functional groups. For this purpose, we designed and synthesized four block co-polymer-based NGs each with a different surface functional group and 10% of the MMT (Figure 4a, Scheme S3 and Figure S6). The surface functional groups include a positively-charged amine group ($NH_2$-NG), an integrin-binding RGD peptide (RGD-NG), a folic acid group (FA-NG), and a control NG (MeO-NG) with no targeting group. All four NGs have their expected charge and have identical sizes based on zeta potential and DLS measurements, respectively (Figure S7). Each NG was incubated separately with HeLa, MCF-7 and HEK293T cells for 24 h, and their uptake was determined using the appropriate response factors (Figure S8). As expected,[67] the FA-NGs were taken up most efficiently in HeLa and MCF-7 cells as these cells over-express folate receptors, whereas the HEK293T cells do not efficiently take up the FA-NGs because they do not over-express the folate receptor (Figure 4b–d). These results indicate that the MMTs can be used to accurately measure the cellular uptake of PNCs. Also, the attached metal has no significant effect on the sensitivity of the measurement.

The key benefit of these MMTs is the ability to quantify the uptake of multiple PNCs in a single experiment. To demonstrate this multiplexing capability in a single experiment, a mixture of equal amounts of MeO-NG, $NH_2$-NG, RGD-NG and FA-NG, each tagged with a different metal ion, was studied. Even though many literature reports demonstrate that these rare earth metal chelates are highly stable in human serum, at low pH (e.g. pH = 0), at high temperature (e.g. 100 °C), and when conjugated to large molecules,[68,69,70] we first tested the ability of the different metals to exchange between the differentially tagged polymers. Polymers each tagged with a different metal ion were placed in separate semi-permeable dialysis tubes (Figure S9). After 24 h, each sample was analyzed by ICP-MS, and we found that no detectable metal exchange occurred between the tubes (Table S1), indicating there is no leakage or 'swapping' of metal ions between the differentially tagged polymers. Confident that each NGs can be measured by its corresponding MMT, we next incubated all four metal-tagged NGs in HeLa, HEK293T and MCF-7 cell cultures. After 24 h, their uptake in this multiplexed experiment was quantified and compared to the uptake of each NG in separate cell cultures (i.e. uniplexed analysis) (Figure 5). The uniplexed and multiplexed analyses provide mostly similar results, indicating that the MMTs can be used to simultaneously evaluate the uptake efficiency of multiple PNCs in a single experiment. In effect, each metal ion (i.e. Tb, Y, Tm, Ho) acts as a proxy for each different NG (i.e. MeO-NG, $NH_2$-NG, RGD-NG, FA-NG). There are some slight differences in uptake observed for the uniplexed and multiplexed experiments, but these differences likely reflect the competition among the four NGs because four times higher concentrations were used in the multiplexed experiment.

## Conclusions

We have demonstrated that MMTs together with ICP-MS analysis can be used to quantify the cellular uptake of PNCs, even in a multiplexed manner. Conjugation of the MMTs to the PNCs has no significant effect on their properties or cellular uptake as long as the percentage of added MMT is kept relatively low (~10%). Moreover, the MMT has no effect on cytotoxicity, suggesting that they should be amenable for *in vivo* analyses. The multiplexed analysis that is possible when multiple metal ions are incorporated allows side-by-side comparisons of different PNCs in the same biological samples, which limits biological variability and reduces analysis time. In future work, we plan to use these MMTs to simultaneously evaluate the *in vivo* biodistributions of multiple PNCs with different properties. The ability to monitor multiple PNCs at the same time will minimize the number of animals needed for these studies, reduce biological variability, and offer a time and cost-efficient method for developing better PNCs for delivery applications.

## Supplementary Material

Refer to Web version on PubMed Central for supplementary material.

## Acknowledgements

R.W.V. acknowledges support from the National Science Foundation (NSF) under grant CHE-2108044. S.T. acknowledges support from the National Institutes of Health (NIH) grant GM-136395.

## References:


(1). Yao Y; Zhou Y; Liu L; Xu Y; Chen Q; Wang Y; Wu S; Deng Y; Zhang J; Shao A Nanoparticle-Based Drug Delivery in Cancer Therapy and Its Role in Overcoming Drug Resistance. Front. Mol. Biosci. 2020, 7 (August), 1–14. 10.3389/fmolb.2020.00193. [PubMed: 32039235]

(2). Narvekar M; Xue HY; Eoh JY; Wong HL Nanocarrier for Poorly Water-Soluble Anticancer Drugs - Barriers of Translation and Solutions. AAPS PharmSciTech 2014, 15 (4), 822–833. 10.1208/s12249-014-0107-x. [PubMed: 24687241]

(3). Pudlarz A; Szemraj J Nanoparticles as Carriers of Proteins, Peptides and Other Therapeutic Molecules. Open Life Sci. 2018, 13 (1), 285–298. 10.1515/biol-2018-0035. [PubMed: 33817095]

(4). Abdifetah O; Na-Bangchang K Pharmacokinetic Studies of Nanoparticles as a Delivery System for Conventional Drugs and Herb-Derived Compounds for Cancer Therapy: A Systematic Review. Int. J. Nanomedicine 2019, 14, 5659–5677. 10.2147/IJN.S213229. [PubMed: 31632004]

(5). Yadav D; Sandeep K; Pandey D; Dutta RK Liposomes for Drug Delivery. J. Biotechnol. Biomater. 2017, 07 (04), 276. 10.4172/2155-952x.1000276.

(6). Sercombe L; Veerati T; Moheimani F; Wu SY; Sood AK; Hua S Advances and Challenges of Liposome Assisted Drug Delivery. Front. Pharmacol. 2015, 6 (DEC), 1–13. 10.3389/fphar.2015.00286. [PubMed: 25805991]

(7). Hong S; Choi DW; Kim HN; Park CG; Lee W; Park HH Protein-Based Nanoparticles as Drug Delivery Systems. Pharmaceutics 2020, 12 (7), 1–28. 10.3390/pharmaceutics12070604.

(8). Martínez-López AL; Pangua C; Reboredo C; Campión R; Morales-Gracia J; Irache JM Protein-Based Nanoparticles for Drug Delivery Purposes. Int. J. Pharm. 2020, 581 (March), 119289. 10.1016/j.ijpharm.2020.119289. [PubMed: 32243968]

(9). Avramović N; Mandić B; Savić-Radojević A; Simić T Polymeric Nanocarriers of Drug Delivery Systems in Cancer Therapy. Pharmaceutics 2020, 12 (4), 1–17. 10.3390/pharmaceutics12040298.

(10). Prabhu RH; Patravale VB; Joshi MD Polymeric Nanoparticles for Targeted Treatment in Oncology: Current Insights. Int. J. Nanomedicine 2015, 10, 1001–1018. 10.2147/IJN.S56932. [PubMed: 25678788]

(11). Han J; Zhao D; Li D; Wang X; Jin Z; Zhao K Polymer-Based Nanomaterials and Applications for Vaccines and Drugs. Polymers (Basel). 2018, 10 (1), 1–14. 10.3390/polym10010031.

(12). Gao J; Wu P; Fernandez A; Zhuang J; Thayumanavan S Cellular AND Gates: Synergistic Recognition to Boost Selective Uptake of Polymeric Nanoassemblies. Angew. Chemie - Int. Ed. 2020, 59 (26), 10456–10460. 10.1002/anie.202002748.

(13). Pugazhendhi A; Edison TNJI; Karuppusamy I; Kathirvel B Inorganic Nanoparticles: A Potential Cancer Therapy for Human Welfare. Int. J. Pharm. 2018, 539 (1–2), 104–111. 10.1016/j.ijpharm.2018.01.034. [PubMed: 29366941]

(14). Sharma A; Goyal AK; Rath G Recent Advances in Metal Nanoparticles in Cancer Therapy. J. Drug Target. 2018, 26 (8), 617–632. 10.1080/1061186X.2017.1400553. [PubMed: 29095640]

(15). Evans ER; Bugga P; Asthana V; Drezek R Metallic Nanoparticles for Cancer Immunotherapy. Mater. Today 2018, 21 (6), 673–685. 10.1016/j.mattod.2017.11.022.

(16). Amiji M; Shenoy D; Kommareddy S Long-Circulating Polymeric Nanoparticles for Drug and Gene Delivery to Tumors. Nanotechnol. Cancer Ther. 2006, No. December, 231–242. 10.1201/9781420006636.ch13.

(17). Alberg I; Kramer S; Schinnerer M; Hu Q; Seidl C; Leps C; Drude N; Möckel D; Rijcken C; Lammers T; Diken M; Maskos M; Morsbach S; Landfester K; Tenzer S; Barz M; Zentel R Polymeric Nanoparticles with Neglectable Protein Corona. Small 2020, 16 (18), 1907574. 10.1002/smll.201907574.

(18). Wei M; Gao Y; Li X; Serpe MJ Stimuli-Responsive Polymers and Their Applications. Polym. Chem. 2017, 8 (1), 127–143. 10.1039/c6py01585a.

(19). Kamaly N; Yameen B; Wu J; Farokhzad OC Degradable Controlled-Release Polymers and Polymeric Nanoparticles: Mechanisms of Controlling Drug Release. Chem. Rev. 2016, 116 (4), 2602–2663. 10.1021/acs.chemrev.5b00346. [PubMed: 26854975]

(20). Li F Controlled Release of Bevacizumab Through Nanospheres for Extended Treatment of Age-Related Macular Degeneration. Open Ophthalmol. J. 2012, 6 (1), 54–58. 10.2174/1874364101206010054. [PubMed: 22798970]

(21). Guo L; Zhang H; Wang F; Liu P; Wang Y; Xia G; Liu R; Li X; Yin H; Jiang H; Chen B Targeted Multidrug-Resistance Reversal in Tumor Based on PEG-PLL-PLGA Polymer Nano Drug Delivery System. Int. J. Nanomedicine 2015, 10, 4535–4547. 10.2147/IJN.S85587. [PubMed: 26213467]

(22). Wilson B; Samanta MK; Santhi K; Kumar KPS; Ramasamy M; Suresh B Chitosan Nanoparticles as a New Delivery System for the Anti-Alzheimer Drug Tacrine. Nanomedicine Nanotechnology, Biol. Med. 2010, 6 (1), 144–152. 10.1016/j.nano.2009.04.001.

(23). Cirstoiu-Hapca A; Buchegger F; Lange N; Bossy L; Gurny R; Delie F Benefit of Anti-HER2-Coated Paclitaxel-Loaded Immuno-Nanoparticles in the Treatment of Disseminated Ovarian Cancer: Therapeutic Efficacy and Biodistribution in Mice. J. Control. Release 2010, 144 (3), 324–331. 10.1016/j.jconrel.2010.02.026. [PubMed: 20219607]

(24). Liu X; Li C; Lv J; Huang F; An Y; Shi L; Ma R Glucose and H2O2 Dual-Responsive Polymeric Micelles for the Self-Regulated Release of Insulin. ACS Appl. Bio Mater. 2020, 3 (3), 1598–1606. 10.1021/acsabm.9b01185.

(25). Li S; Zhang Y; Ho SH; Li B; Wang M; Deng X; Yang N; Liu G; Lu Z; Xu J; Shi Q; Han JY; Zhang L; Wu Y; Zhao Y; Nie G Combination of Tumour-Infarction Therapy and Chemotherapy via the Co-Delivery of Doxorubicin and Thrombin Encapsulated in Tumour-Targeted Nanoparticles. Nat. Biomed. Eng. 2020, 4 (7), 732–742. 10.1038/s41551-020-0573-2. [PubMed: 32572197]

(26). Yang Y; Li Y; Chen K; Zhang L; Qiao S; Tan G; Chen F; Pan W Dual Receptor-Targeted and Redox-Sensitive Polymeric Micelles Self-Assembled from a Folic Acid-Hyaluronic Acid-SS-Vitamin E Succinate Polymer for Precise Cancer Therapy. Int. J. Nanomedicine 2020, 15, 2885–2902. 10.2147/IJN.S249205. [PubMed: 32425522]

(27). Pereira P; Correia A; Gama FM In Vivo Imaging of Glycol Chitosan-Based Nanogel Biodistribution. Macromol. Biosci. 2016, 16 (3), 432–440. 10.1002/mabi.201500267. [PubMed: 26663610]

(28). Gordon MR; Zhuang J; Ventura J; Li L; Raghupathi K; Thayumanavan S Biodistribution Analysis of NIR-Labeled Nanogels Using in Vivo FMT Imaging in Triple Negative Human Mammary Carcinoma Models. Mol. Pharm. 2018, 15 (3), 1180–1191. 10.1021/acs.molpharmaceut.7b01011. [PubMed: 29378144]

(29). Lux J; White AG; Chan M; Anderson CJ; Almutairi A Nanogels from Metal-Chelating Crosslinkers as Versatile Platforms Applied to Copper-64 PET Imaging of Tumors and Metastases. Theranostics 2015, 5 (3), 277–288. 10.7150/thno.10904. [PubMed: 25553115]

(30). Rossin R; Muro S; Welch MJ; Muzykantov VR; Schustery DP In Vivo Imaging of 64 Cu-Labeled Polymer Nanoparticles Targeted to the Lung Endothelium. J. Nucl. Med. 2008, 49 (1), 103–111. 10.2967/jnumed.107.045302. [PubMed: 18077519]

(31). Wu S; Helal-Neto E; Matos A. P. dos S.; Jafari A; Kozempel J; Silva Y. J. de A.; Serrano-Larrea C; Alves Junior S; Ricci-Junior E; Alexis F; Santos-Oliveira R Radioactive Polymeric Nanoparticles for Biomedical Application. Drug Deliv. 2020, 27 (1), 1544–1561. 10.1080/10717544.2020.1837296. [PubMed: 33118416]

(32). Jackson AW; Chandrasekharan P; Shi J; Rannard SP; Liu Q; Yang CT; He T Synthesis and in Vivo Magnetic Resonance Imaging Evaluation of Biocompatible Branched Copolymer Nanocontrast Agents. Int. J. Nanomedicine 2015, 10, 5895–5907. 10.2147/IJN.S88764. [PubMed: 26425088]

(33). Zhang C; Moonshi SS; Wang W; Ta HT; Han Y; Han FY; Peng H; Král P; Rolfe BE; Gooding JJ; Gaus K; Whittaker AK High F-Content Perfluoropolyether-Based Nanoparticles for Targeted Detection of Breast Cancer by 19F Magnetic Resonance and Optical Imaging. ACS Nano 2018, 12 (9), 9162–9176. 10.1021/acsnano.8b03726. [PubMed: 30118590]

(34). Obinu A; Gavini E; Rassu G; Riva F; Calligaro A; Bonferoni MC; Maestri M; Giunchedi P Indocyanine Green Loaded Polymeric Nanoparticles: Physicochemical Characterization and Interaction Studies with Caco-2 Cell Line by Light and Transmission Electron Microscopy. Nanomaterials 2020, 10 (1), 133. 10.3390/nano10010133.

(35). Reifarth M; Hoeppener S; Schubert US Uptake and Intracellular Fate of Engineered Nanoparticles in Mammalian Cells: Capabilities and Limitations of Transmission Electron Microscopy—Polymer-Based Nanoparticles. Adv. Mater. 2018, 30 (9), 1–28. 10.1002/adma.201703704.

(36). Chen S; Xiong C; Liu H; Wan Q; Hou J; He Q; Badu-Tawiah A; Nie Z Mass Spectrometry Imaging Reveals the Sub-Organ Distribution of Carbon Nanomaterials. Nat. Nanotechnol. 2015, 10 (2), 176–182. 10.1038/nnano.2014.282. [PubMed: 25652170]

(37). Fülöp A; Sammour DA; Erich K; Von Gerichten J; Van Hoogevest P; Sandhoff R; Hopf C Molecular Imaging of Brain Localization of Liposomes in Mice Using MALDI Mass Spectrometry. Sci. Rep. 2016, 6, 1–10. 10.1038/srep33791. [PubMed: 28442746]

(38). Christensen J; Litherland K; Faller T; Van De Kerkhof E; Natt F; Hunziker J; Boos J; Beuvink I; Bowman K; Baryza J; Beverly M; Vargeese C; Heudi O; Stoeckli M; Krauser J; Swart P Biodistribution and Metabolism Studies of Lipid Nanoparticle- Formulated Internally [3H]-Labeled SiRNA in Mices. Drug Metab. Dispos. 2014, 42 (3), 431–440. 10.1124/dmd.113.055434. [PubMed: 24389421]

(39). Xue J; Liu H; Chen S; Xiong C; Zhan L; Sun J; Nie Z Mass Spectrometry Imaging of the in Situ Drug Release from Nanocarriers. Sci. Adv. 2018, 4 (10), eaat9039. 10.1126/sciadv.aat9039. [PubMed: 30402541]

(40). Hou S; Sikora KN; Tang R; Liu Y; Lee YW; Kim ST; Jiang Z; Vachet RW; Rotello VM Quantitative Differentiation of Cell Surface-Bound and Internalized Cationic Gold Nanoparticles Using Mass Spectrometry. ACS Nano 2016, 10 (7), 6731–6736. 10.1021/acsnano.6b02105. [PubMed: 27337000]

(41). Zhu ZJ; Ghosh PS; Miranda OR; Vachet RW; Rotello VM Multiplexed Screening of Cellular Uptake of Gold Nanoparticles Using Laser Desorption/Ionization Mass Spectrometry. J. Am. Chem. Soc. 2008, 130 (43), 14139–14143. 10.1021/ja805392f. [PubMed: 18826222]

(42). Yan B; Kim ST; Kim CS; Saha K; Moyano DF; Xing Y; Jiang Y; Roberts AL; Alfonso FS; Rotello VM; Vachet RW Multiplexed Imaging of Nanoparticles in Tissues Using Laser Desorption/Ionization Mass Spectrometry. J. Am. Chem. Soc. 2013, 135 (34), 12564–12567. 10.1021/ja406553f. [PubMed: 23931011]

(43). Elci SG; Jiang Y; Yan B; Kim ST; Saha K; Moyano DF; Yesilbag Tonga G; Jackson LC; Rotello VM; Vachet RW Surface Charge Controls the Suborgan Biodistributions of Gold Nanoparticles. ACS Nano 2016, 10 (5), 5536–5542. 10.1021/acsnano.6b02086. [PubMed: 27164169]

(44). Hsiao IL; Bierkandt FS; Reichardt P; Luch A; Huang YJ; Jakubowski N; Tentschert J; Haase A Quantification and Visualization of Cellular Uptake of TiO2 and Ag Nanoparticles: Comparison of Different ICP-MS Techniques. J. Nanobiotechnology 2016, 14 (1), 1–13. 10.1186/s12951-016-0203-z. [PubMed: 26743777]

(45). Goto-Inoue N; Hayasaka T; Zaima N; Setou M Imaging Mass Spectrometry for Lipidomics. Biochim. Biophys. Acta - Mol. Cell Biol. Lipids 2011, 1811 (11), 961–969. 10.1016/j.bbalip.2011.03.004.

(46). Liu C; Yu D; Ge F; Yang L; Wang Q Fluorescent and Mass Spectrometric Evaluation of the Phagocytic Internalization of a CD47-Peptide Modified Drug-Nanocarrier. Anal. Bioanal. Chem. 2019, 411 (18), 4193–4202. 10.1007/s00216-019-01825-y. [PubMed: 31093697]

(47). Han G; Spitzer MH; Bendall SC; Fantl WJ; Nolan GP Metal-Isotope-Tagged Monoclonal Antibodies for High-Dimensional Mass Cytometry. Nat. Protoc. 2018, 13 (10), 2121–2148. 10.1038/s41596-018-0016-7. [PubMed: 30258176]

(48). Schwarz G; Mueller L; Beck S; Linscheid MW DOTA Based Metal Labels for Protein Quantification: A Review. J. Anal. At. Spectrom. 2014, 29 (2), 221–233. 10.1039/c3ja50277e.

(49). Lou X; Zhang G; Herrera I; Kinach R; Ornatsky O; Baranov V; Nitz M; Winnik MA Polymer-Based Elemental Tags for Sensitive Bioassays. Angew. Chemie - Int. Ed. 2007, 46 (32), 6111–6114. 10.1002/anie.200700796.

(50). Spitzer MH; Nolan GP Mass Cytometry: Single Cells, Many Features. Cell 2016, 165 (4), 780–791. 10.1016/j.cell.2016.04.019. [PubMed: 27153492]

(51). Giesen C; Wang HAO; Schapiro D; Zivanovic N; Jacobs A; Hattendorf B; Schüffler PJ; Grolimund D; Buhmann JM; Brandt S; Varga Z; Wild PJ; Günther D; Bodenmiller B Highly

Multiplexed Imaging of Tumor Tissues with Subcellular Resolution by Mass Cytometry. Nat. Methods 2014, 11 (4), 417–422. 10.1038/nmeth.2869. [PubMed: 24584193]

(52). Chang Q; Ornatsky OI; Siddiqui I; Loboda A; Baranov VI; Hedley DW Imaging Mass Cytometry. Cytom. Part A 2017, 91 (2), 160–169. 10.1002/cyto.a.23053.

(53). Baharlou H; Canete NP; Cunningham AL; Harman AN; Patrick E Mass Cytometry Imaging for the Study of Human Diseases—Applications and Data Analysis Strategies. Front. Immunol. 2019, 10 (November), 1–22. 10.3389/fimmu.2019.02657. [PubMed: 30723466]

(54). Reeßing F; Stuart MCA; Samplonius DF; Dierckx RAJO; Feringa BL; Helfrich W; Szymanski W A Light-Responsive Liposomal Agent for MRI Contrast Enhancement and Monitoring of Cargo Delivery. Chem. Commun. 2019, 55 (72), 10784–10787. 10.1039/c9cc05516a.

(55). Tong G; Fang Z; Huang G; Jing Y; Dai S; Jiang Q; Zhang C; Feng ST; Li ZP Gadolinium/DOTA Functionalized Poly(Ethylene Glycol)-: Block -Poly(Acrylamide-Co -Acrylonitrile) Micelles with Synergistically Enhanced Cellular Uptake for Cancer Theranostics. RSC Adv. 2016, 6 (56), 50534–50542. 10.1039/c6ra04038a.

(56). Tang J; Sheng Y; Hu H; Shen Y Macromolecular MRI Contrast Agents: Structures, Properties and Applications. Prog. Polym. Sci. 2013, 38 (3–4), 462–502. 10.1016/j.progpolymsci.2012.07.001.

(57). Liu Z; Cai W; He L; Nakayama N; Chen K; Sun X; Chen X; Dai H In Vivo Biodistribution and Highly Efficient Tumour Targeting of Carbon Nanotubes in Mice. Nat. Nanotechnol. 2007, 2 (1), 47–52. 10.1038/nnano.2006.170. [PubMed: 18654207]

(58). Stockhofe K; Postema JM; Schieferstein H; Ross TL Radiolabeling of Nanoparticles and Polymers for PET Imaging. Pharmaceuticals 2014, 7 (4), 392–418. 10.3390/ph7040392. [PubMed: 24699244]

(59). Gao J; Dutta K; Zhuang J; Thayumanavan S Cellular- and Subcellular-Targeted Delivery Using a Simple All-in-One Polymeric Nanoassembly. Angew. Chemie 2020, 132 (52), 23672–23676. 10.1002/ange.202008272.

(60). Wu P; Gao J; Prasad P; Dutta K; Kanjilal P; Thayumanavan S Influence of Polymer Structure and Architecture on Drug Loading and Redox-Triggered Release. Biomacromolecules 2022, 23 (1), 339–348. 10.1021/acs.biomac.1c01295. [PubMed: 34890192]

(61). Jiang Z; Liu H; He H; Ribbe AE; Thayumanavan S Blended Assemblies of Amphiphilic Random and Block Copolymers for Tunable Encapsulation and Release of Hydrophobic Guest Molecules. Macromolecules 2020, 53 (7), 2713–2723. 10.1021/acs.macromol.9b02595.

(62). Dutta K; Bochicchio D; Ribbe AE; Alfandari D; Mager J; Pavan GM; Thayumanavan S Symbiotic Self-Assembly Strategy toward Lipid-Encased Cross-Linked Polymer Nanoparticles for Efficient Gene Silencing. ACS Appl. Mater. Interfaces 2019, 11 (28), 24971–24983. 10.1021/acsami.9b04731. [PubMed: 31264399]

(63). Dutta K; Hu D; Zhao B; Ribbe AE; Zhuang J; Thayumanavan S Templated Self-Assembly of a Covalent Polymer Network for Intracellular Protein Delivery and Traceless Release. J. Am. Chem. Soc. 2017, 139 (16), 5676–5679. 10.1021/jacs.7b01214. [PubMed: 28406017]

(64). Anson F; Liu B; Kanjilal P; Wu P; Hardy JA; Thayumanavan S Evaluating Endosomal Escape of Caspase-3-Containing Nanomaterials Using Split GFP. Biomacromolecules 2021, 22 (3), 1261–1272. 10.1021/acs.biomac.0c01767. [PubMed: 33591168]

(65). Ryu JH; Chacko RT; Jiwpanich S; Bickerton S; Babu RP; Thayumanavan S Self-Cross-Linked Polymer Nanogels: A Versatile Nanoscopic Drug Delivery Platform. J. Am. Chem. Soc. 2010, 132 (48), 17227–17235. 10.1021/ja1069932. [PubMed: 21077674]

(66). Jiang Z; He H; Liu H; Thayumanavan S Cellular Uptake Evaluation of Amphiphilic Polymer Assemblies: Importance of Interplay between Pharmacological and Genetic Approaches. Biomacromolecules 2019, 20 (12), 4407–4418. 10.1021/acs.biomac.9b01073. [PubMed: 31609589]

(67). Ryu JH; Bickerton S; Zhuang J; Thayumanavan S Ligand-Decorated Nanogels: Fast One-Pot Synthesis and Cellular Targeting. Biomacromolecules 2012, 13 (5), 1515–1522. 10.1021/bm300201x. [PubMed: 22455467]

(68). Frenzel T; Lengsfeld P; Schirmer H; Hütter J; Weinmann HJ Stability of Gadolinium-Based Magnetic Resonance Imaging Contrast Agents in Human Serum at 37°C. Invest. Radiol. 2008, 43 (12), 817–828. 10.1097/RLI.0b013e3181852171. [PubMed: 19002053]

(69). Yokoyama M; Shiraishi K Stability Evaluation of Gd Chelates for Macromolecular MRI Contrast Agents. Magn. Reson. Mater. Physics, Biol. Med. 2020, 33 (4), 527–536. 10.1007/s10334-019-00805-8.

(70). Ahrends R; Pieper S; Neumann B; Scheler C; Linscheid MW Metal-Coded Affinity Tag Labeling: A Demonstration of Analytical Robustness and Suitability for Biological Applications. Anal. Chem. 2009, 81 (6), 2176–2184. 10.1021/ac802310c. [PubMed: 19228048]

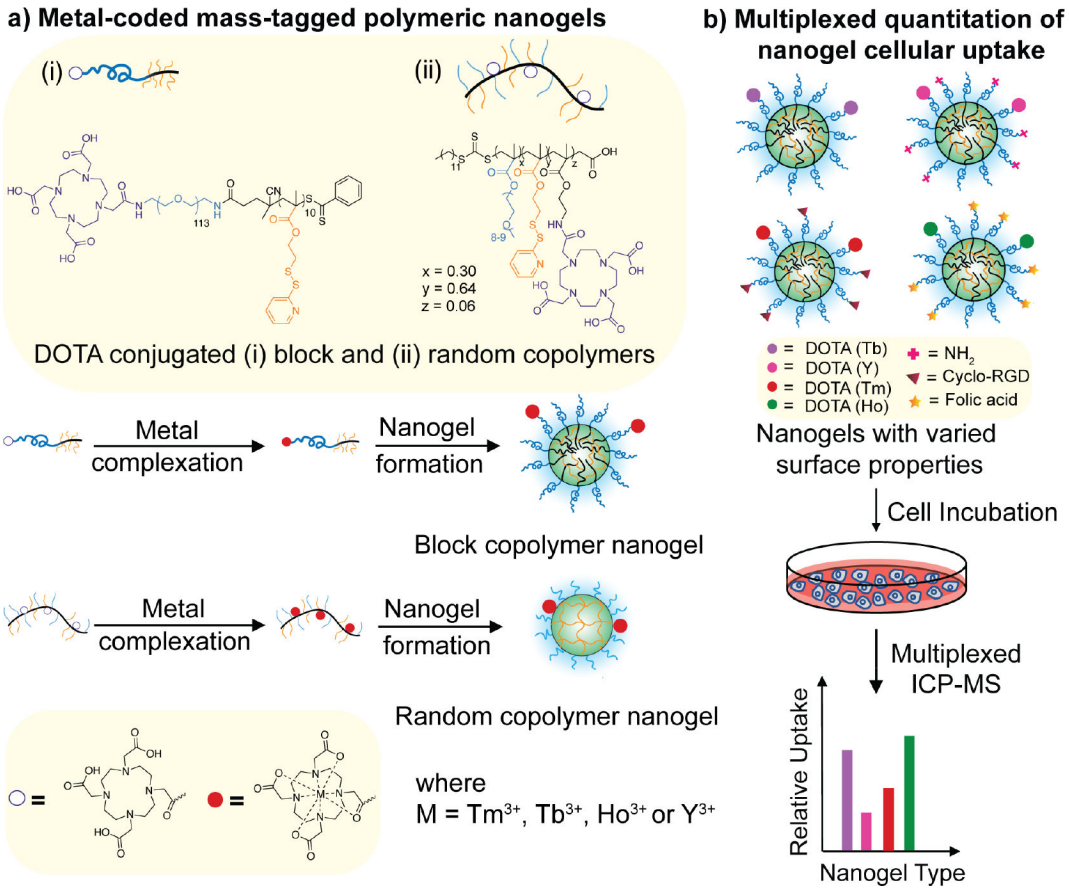


**Figure 1.**

Metal-coded mass tagged polymeric nanogels for multiplexed quantitative measurements of cellular uptake. (a) Structures of polymeric nanogels studied in this work. (b) Workflow for analyzing the cellular uptake of multiple nanogels with different targeting groups in a single experiment using ICP-MS.

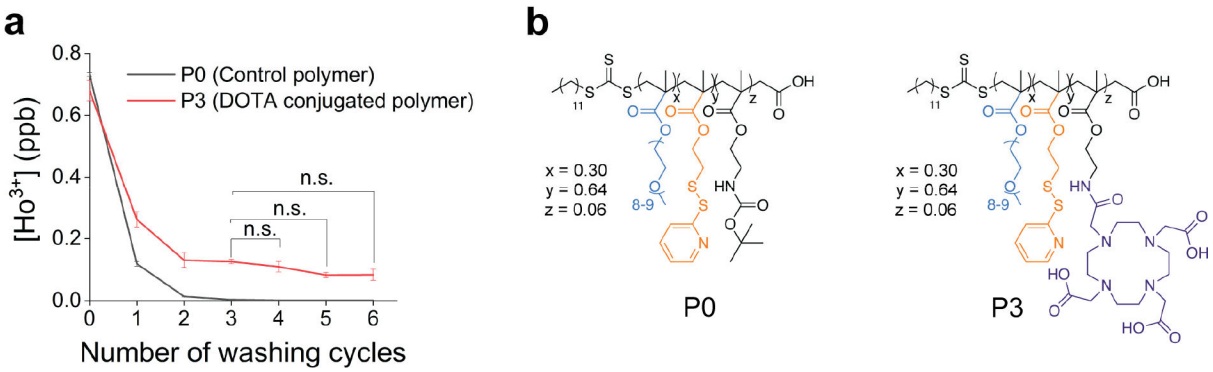


**Figure 2.**

(a) ICP-MS analysis after $Ho^{3+}$ complexation of P3 and the control polymer P0 for a different number of washing cycles. Three washing steps were enough to remove free, non-specifically bound $Ho^{3+}$, as indicated by the undetectable levels of $Ho^{3+}$ in P0. The abbreviation n.s. indicates no significant difference in the signals. (b) Chemical structures of control polymer (i.e. P0) and DOTA conjugated polymer (i.e. P3).

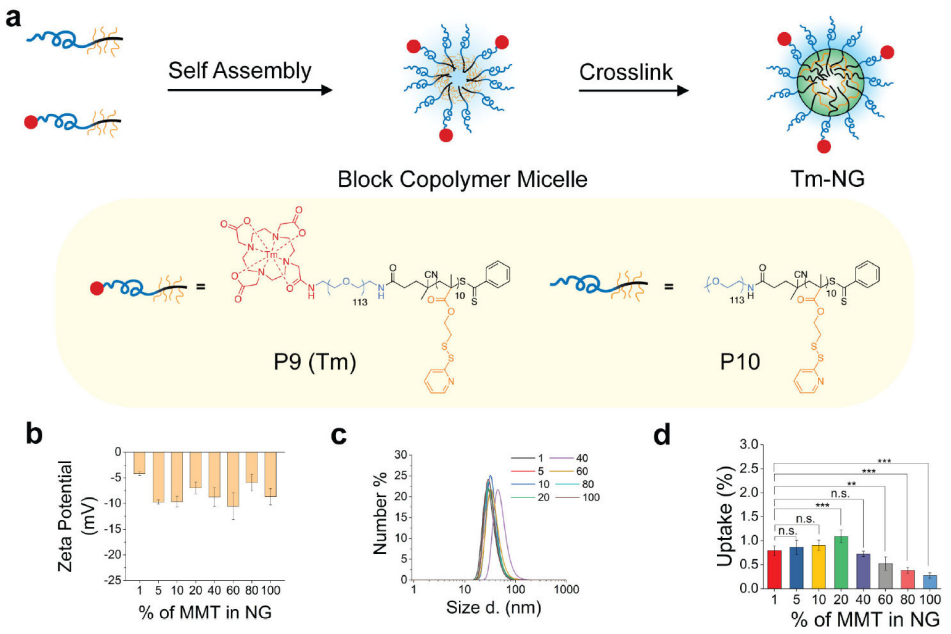


**Figure 3.**

Optimization of MMT density on the NGs. (a) Schematic illustrating the fabrication of NGs with varying MMT densities. (b) Zeta potentials of NGs with different MMT densities, showing little effect on surface charge. (c) DLS profiles of NGs, illustrating no effect of MMT density onto NG size. (d) ICP-MS quantification of NG uptake in HeLa cells. Up to 10% MMT can be incorporated into the NGs without significantly altering uptake.

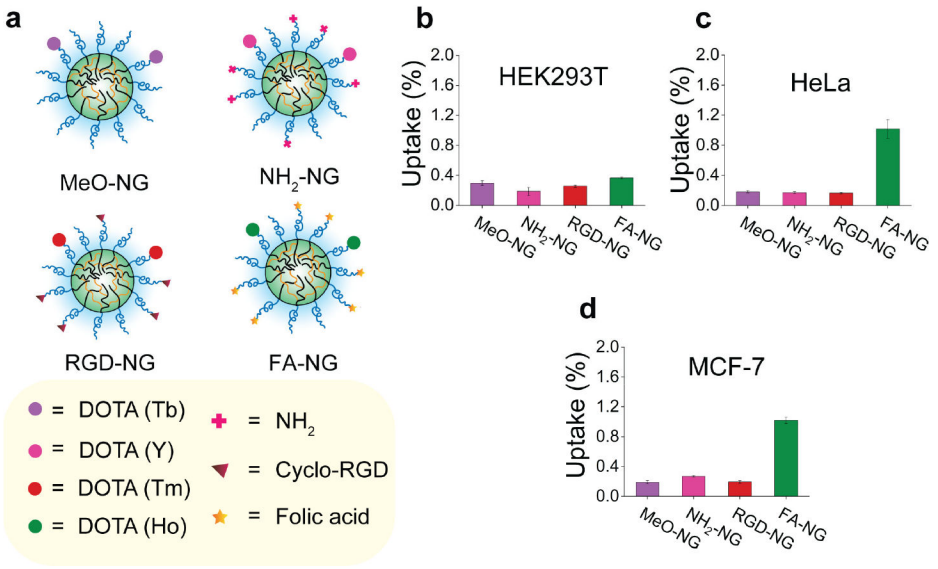


**Figure 4.**

Validation of cellular-uptake quantification using the MMT PNCs. (a) Schematic of NGs with different surface targeting ligands and MMTs with different complexed metal ions (Scheme S3 and Figure S6). ICP-MS measurements of NG uptake in (b) HEK293T, (c) HeLa, and (d) MCF-7 cells. FA-functionalized NGs are taken up to a greater extent in HeLa and MCF-7 cells than other NGs because HeLa and MCF-7 cells have high concentrations of folate receptors.

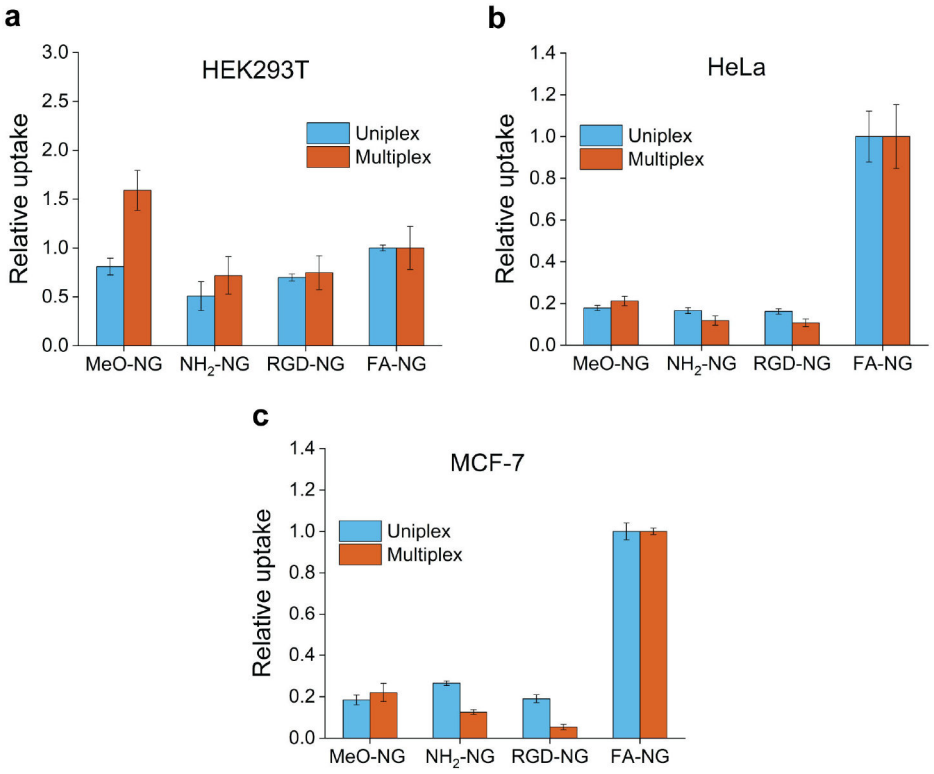


**Figure 5.**

Multiplexed screening of the cellular uptake of multiple NGs in a single experiment and comparisons to individual uptake experiments (i.e. uniplex). A mixture of equal amounts of all four NGs was spiked separately into (a) HEK293T, (b) HeLa, and (c) MCF-7 cells. After 24 h of incubation, uptake of all four NGs was quantified in a single experiment (i.e. multiplex). The multiplexed analysis resulted in similar relative uptake of the NGs as obtained in uniplexed analyses where each NG was spiked individually into the cells.